THE JOURNAL OF PHYSICAL CHEMISTRY Letters

Letter

Cite This: J. Phys. Chem. Lett. 2018, 9, 3049−3056

pubs.acs.org/JPCL

Tuning Solvated Electrons by Polar−Nonpolar Oxide Heterostructure

Yanan Wang,[†] Hongli Guo,[†,‡] Qijing Zheng,*[,†] Wissam A. Saidi,[§] and Jin Zhao*[,†,∥,⊥]

[†]ICQD/Hefei National Laboratory for Physical Sciences at Microscale and Key Laboratory of Strongly-Coupled Quantum Matter Physics, Chinese Academy of Sciences and Department of Physics, University of Science and Technology of China, Hefei, Anhui 230026, China

[‡]School of Physics and Technology, Center for Nanoscience and Nanotechnology, and Key Laboratory of Artificial Micro- and Nano-structures of Ministry of Education, Wuhan University, Wuhan 430072, China

[§]Department of Mechanical Engineering and Materials Science, University of Pittsburgh, Pittsburgh, Pennsylvania 15261, United States

[∥]Department of Physics and Astronomy, University of Pittsburgh, Pittsburgh, Pennsylvania 15260, United States

[⊥]Synergetic Innovation Center of Quantum Information & Quantum Physics, University of Science and Technology of China, Hefei, Anhui 230026, China

Supporting Information

ABSTRACT: Solvated electron states at the oxide/aqueous interface represent the lowest energy charge-transfer pathways, thereby playing an important role in photocatalysis and electronic device applications. However, their energies are usually higher than the conduction band minimum (CBM), which makes the solvated electrons difficult to utilize in charge-transfer processes. Thus it is essential to stabilize the energy of the solvated electron states. Taking $LaAlO_3/SrTiO_3$ (LAO/STO) oxide heterostructure with H_2O-adsorbed monolayer as a prototypical system, we show using DFT and ab initio time-dependent nonadiabatic molecular dynamics simulation that the energy and dynamics of solvated electrons can be tuned by the electric field in the polar−nonpolar oxide heterostructure. In particular, for LAO/STO with p-type interface, the CBM is contributed by the solvated electron state when LAO is thicker than four unit cells. Furthermore, the solvated electron band minimum can be partially occupied when LAO is thicker than eight unit cells. We propose that the tunability of solvated electron states can be achieved on polar−nonpolar oxide heterostructure surfaces as well as on ferroelectric oxides, which is important for charge and proton transfer at oxide/aqueous interfaces.

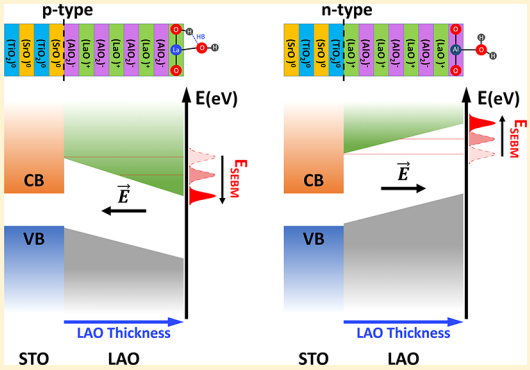

Solvated electron, which can be stabilized in a solvent by polarizing its surrounding, is one of the most fundamental chemical reagents of intense experimental and theoretical interest.[1−28] Since their discovery in intense blue coloration in solutions of alkali metals in ammonia, solvated electrons have been found to be important negative charge carriers that are also closely related to proton transfer.[29−39] Therefore, the investigation on solvated electrons has significance in physics, chemistry, and biology.

Most experimental and theoretical investigations of solvated electrons have focused on elucidating their equilibrium structure and solvation dynamics in a variety of neat liquids.[1−5,7,9−13,15,17,19,20,36,38,40−44] It is well established that an excess electron can be bound by dipolar forces to surfaces of small H_2O clusters.[45−47] Ab initio calculations show that such partially hydrated or "wet" electrons on clusters are bound to the "dangling" H atoms, which do not form strong hydrogen bonds (HBs).[1,4,6,45,46] The dynamics of such solvated, dubbed "wet" electrons are intensively studied.[2,5,7,9−12,14−16,18−20,30,34,35,39]

More interestingly, the nature of the solid−liquid interfacial solvated electrons is of great importance to the fields of electrochemistry, catalysis, geochemistry, and solar energy conversion.[6,8,29,31,48−52] For example, solvated electrons at TiO_2/aqueous interface are proposed to be an important medium for photocatalysis.[6,8,31,53−55] Interfacial solvated electron states were initially observed at the H_2O/TiO_2 interface by time-resolved two-photon photoemission (TR-2PPE).[6,8] Furthermore, at the CH_3OH/TiO_2 interface, the solvated electron states and related proton-coupled electron transfer are observed by experiments and investigated by a different level of theoretical methods.[31,53,56−58] Similar to solvated electrons in liquids, the solvated electrons on the solid surface are also stabilized by dangling hydrogen atoms.[6,8,53−55] The difference is that because solid surfaces contribute additional electronic states, the solvated electron states on

Received: March 27, 2018
Accepted: May 16, 2018
Published: May 16, 2018

Downloaded via ZHEJIANG UNIV on July 13, 2026 at 03:07:06 (UTC).
See https://pubs.acs.org/sharingguidelines for options on how to legitimately share published articles.

© 2018 American Chemical Society

DOI: 10.1021/acs.jpclett.8b00938
J. Phys. Chem. Lett. 2018, 9, 3049−3056

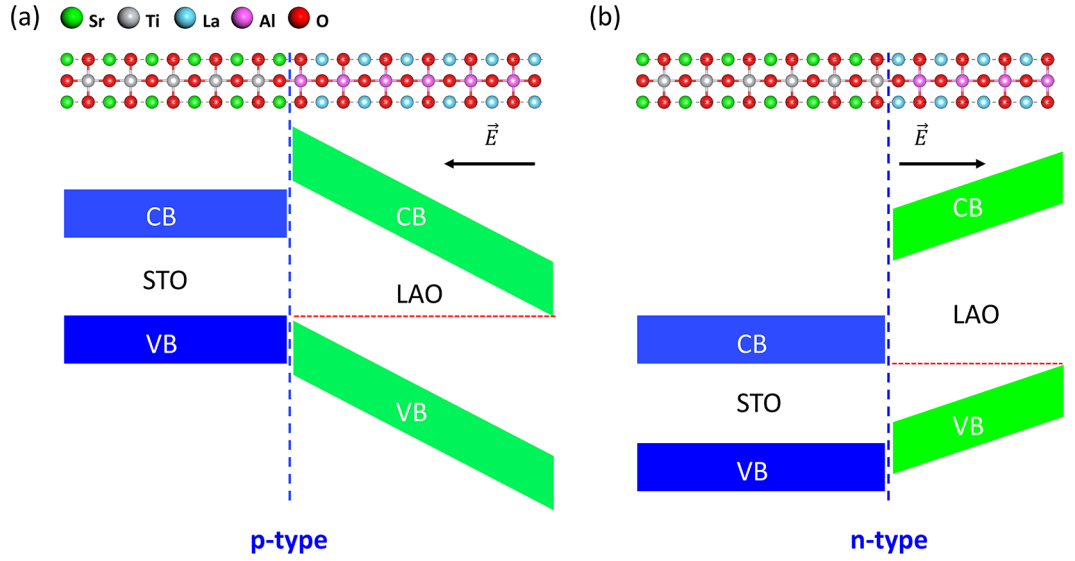

Figure 1. Atomic structure and schematic map of the electric potential of LAO/STO heterostructure: (a) p-type with six uc's LAO and (b) n-type with four uc's LAO. The red dashed lines indicate the position of VBM.

solid surfaces usually exist as excited states with a certain lifetime. For example, the injection and trapping of electrons in multilayer amorphous and crystalline ice on metal surfaces have been studied by time-resolved photoemission techniques.[18,48−52] The hydration of electrons photoinjected from metals into the conduction band of ice proceeds on time scales that span more than 15 orders of magnitude.[49] On metal oxide surfaces, the interaction between the adsorbed molecules with the substrate is stronger, which makes the lifetime of the solvated electrons relatively short.[6,8] For example, at the H_2O/TiO_2 interface, the lifetime is measured to be as short as 10−14 fs.[6] Such a short lifetime hinders photochemical reactions.

Therefore, to realize the applications of solvated electrons in photocatalysis and charge transport, it is important to stabilize the solvated electrons and increase their lifetime. Previous investigations showed that solvated electrons can be stabilized by increasing the number of dangling HBs and the interface dipole moment.[54,55] Nevertheless, on TiO_2 surfaces, the solvated electron state is still as high as 1.8 eV above the CBM, even when a 1D dangling hydrogen chain is formed with one monolayer (ML) of H adsorbates.[54] How to stabilize the solvated electron states close to CBM or even the Fermi level (E_F) is still an important and unsolved problem.

Using first-principles calculations, we propose a strategy to stabilize the solvated electron states using the built-in electric field in the polar−nonpolar oxide heterostructure such as LAO/STO.[59−76] We investigate the solvated electron states of one ML H_2O adsorbed on LAO/STO surface. It is found that the energy of the solvated electron states in H_2O can be significantly tuned by the built-in electric field in LAO. We find that the solvated electron states on LAO/STO with n-type interface are pushed away from CBM. With different thickness of LAO, the solvated electron band minimum (SEBM) can be tuned from 2.1 to 4.0 eV above CBM. In contrast, on LAO/STO with p-type interface, where the electric field in LAO is in the opposite direction compared with n-type interface, the solvated electron states can be stabilized toward the Fermi energy. Namely, we find that the energy of SEBM decreases with the increase in the electric potential along with the LAO thickness, which can be tuned from 3.6 to −0.03 eV according to valence band maximum (VBM). Before LAO thickness reaches four unit cells (uc's), SEBM is higher than CBM with a lifetime around 15 fs. After LAO reaches four uc's, the CBM is contributed by the SEBM. Moreover, the SEBM can be further stabilized and partially occupied when the LAO thickness reaches eight uc's. The results are expected to be general and applicable to other polar−nonpolar oxide heterostructures as well as ferroelectric systems, which provide an efficient way to tune the energy of solvated electrons and achieve their applications in photocatalysis and charge transport at oxide/aqueous interfaces.

Plane-wave pseudopotential DFT calculations are used to characterize H_2O molecules adsorbed on the surface of LAO/STO (001). The calculations are carried out with the "Vienna ab initio simulation package" (VASP) code.[77−79] The Perdew−Burke−Ernzerhof (PBE) functional with generalized gradient approximation (GGA) is employed for the geometry optimization and the electronic structure calculations.[80] The projector-augmented wave method is used to describe the ion−electron interactions.[81] An energy cutoff of 500 eV is employed. The atomic structures are relaxed using a conjugate gradient scheme without any symmetry restrictions until the maximum ionic force on each of them is <0.02 eV $Å^{-1}$. The periodically repeated slabs are decoupled by 15 Å vacuum gaps, and in-plane lattice constant is fixed at 3.905 Å. A Monkhorst−Pack grid of (9 × 9 × 1) k-points is set for the (1 × 1) surface unit cell. To explore the solvated electron states on the surface of LAO/STO, we introduce one ML H_2O adsorbed on the surfaces. The slab contains six STO uc's in which the lower two uc's are fixed to the bulk configuration while the upper four STO uc's are allowed to relax together with LAO and H_2O. The solvated electron state is determined by plotting the 1D orbital distribution perpendicular to the slab. If the orbital distribution is >60% localized on the H_2O layer, then it is determined as a solvated electron state.

The excited solvated electron dynamics on p-type of LAO/STO with one to three uc LAO are investigated using time-dependent ab initio nonadiabatic molecular dynamics (NAMD) simulation using Hefei-NAMD code,[82,83] which augments the VASP with the NAMD capabilities within time-dependent

DOI: 10.1021/acs.jpclett.8b00938
J. Phys. Chem. Lett. 2018, 9, 3049−3056

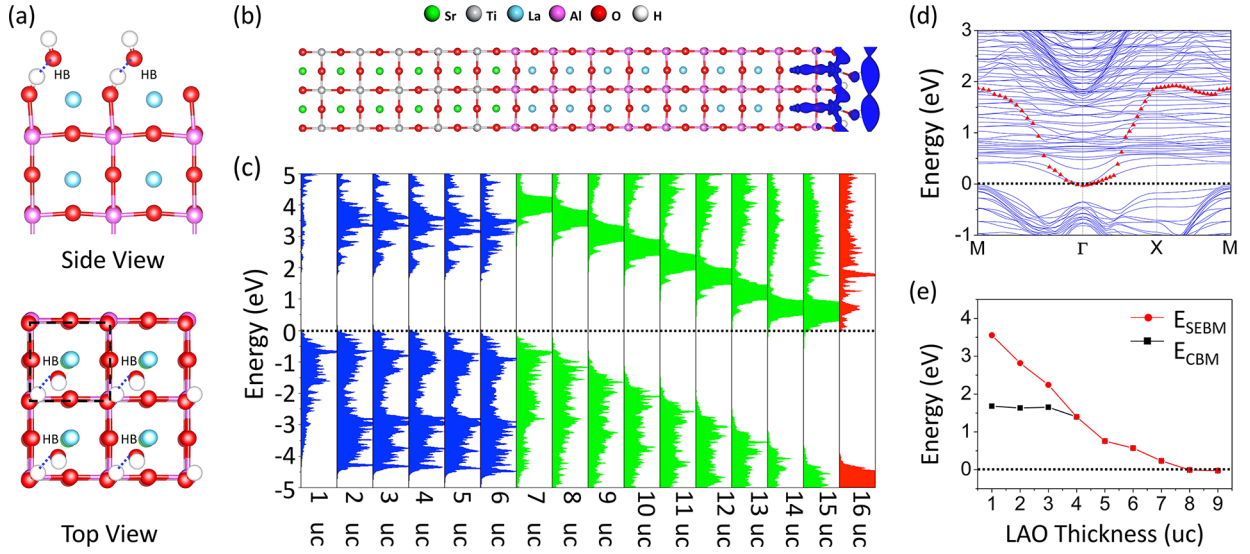

Figure 2. (a) Side and top views of one ML H_2O adsorbed on p-type LAO/STO heterostructure. (b) Spatial orbital distribution of the solvated state in H_2O layer. (c) Layer-resolved DOS for every LAO, STO, and H_2O layer, represented by green, blue, and red. The dashed line represents the position of E_F. (d) Band structure of one ML H_2O adsorbed on p-type LAO/STO. The solvated electron band is marked by red triangles. (e) Dependence of SEBM and CBM energies on LAO thickness. The energy of VBM is set as the reference in panels c–e. The results in panels a–d correspond to one ML H_2O adsorbed on p-type LAO/STO with nine uc's LAO. The E_F and VBM are very close in energy in panels c and d.

density functional theory (TDDFT) similar to refs 84–86. After geometry optimization, we use velocity rescaling to bring the temperature of the system to 50 K. A 5 ps microcanonical ab initio molecular dynamics trajectory is then generated using a 1 fs time step. The NAMD results are obtained by averaging over 100 different initial configurations selected from the MD trajectory based on the classical path approximation.[56] For each chosen structure, we sample 2×10^4 trajectories of the last 2 ps. More details are included in the Supporting Information.

Heterostructures composed of perovskite oxides such as STO and LAO, epitaxially stacked along the (001) direction have generated a lot of interest in recent years.[59−73] The exciting properties stem from the polar–nonpolar nature of LAO/STO, as can be seen by examining the nominal charges of the layers, which are +1 (LaO) and −1 (AlO_2) in LAO (001) layers and neutral for the TiO_2 and SrO layers of STO (001). Hence in LAO (001)/STO(001) heterostructures there are two possible interfaces, namely, n-type $(LaO)^+/(TiO_2)^0$ and p-type $(AlO_2)^-/(SrO)^0$, as shown in Figure 1a,b. The electric fields in n and p types LAO/STO heterostructures are in opposite directions.

Because of the polar nature of LAO, the potential across each LAO uc is additive and diverges linearly with the thickness of the LAO film. This phenomenon is known as "polar catastrophe".[59,63,66,68,69] To offset the diverging potential, an electronic reconstruction is expected to occur by transferring half an electron (hole) to the n-type (p-type) interface. This charge transfer can lead to an insulating-to-metallic transition. Our results show that an insulating-to-metallic transition will take place for LAO films thicker than six and four uc's for p-type and n-type LAO/STO, respectively, as schematically shown in Figure 1. This agrees with our previous study as well as other investigations.[62] We propose to tune the energy of the solvated electron states using the electric field in LAO films of these two types of heterostructures.

First, we investigate the solvated electrons of one ML H_2O adsorbed on LAO/STO heterostructure with p-type interface with LaO termination. Our results show that the optimized H_2O adsorption structures do not exhibit significant dependence on the LAO thickness. Figure 2a–d shows the atomic and electronic structures of one ML H_2O adsorbed on LAO/STO with nine uc's LAO. H_2O dissociates into one OH on La atom and one H on O atom without energy barrier. The adsorption energy is 0.93 eV. The dissociated H and the OH form a strong HB with a bond length of 1.55 Å. Thus only the H in OH behaves as a dangling H atom, which can bind the solvated electrons. The OH on the La atom is nearly perpendicular to the surface, which induces a vertical dipole moment that can further stabilize the solvated electrons. The solvated electron states of one ML H_2O on LAO/STO surface form an electronic band shown by red triangles in Figure 2d, and the SEBM spatial orbital distribution is plotted in Figure 2b. It can be seen that the solvated electron states hybridize with the substrate, similar to H_2O and CH_3OH frontiers levels on TiO_2.[57,58,87,88] One can see that the solvated electron states are mainly stabilized by the upper dangling hydrogen atoms of H_2O layer. Such states show diffusive character and form a dispersive band, as shown in Figure 2d. The effective mass at SEBM is $m^* = 1.19m_e$, which is close to the effective mass of a free electron (m_e), suggesting that such a solvated electron band is ideal for electron conduction. The band structure (Figure 2d) or the layer-resolved DOS (Figure 2c) shows that the SEBM is located 0.03 eV below E_F, which means the solvated electron band is partially occupied.

The stabilization of solvated electron band is due to the built-in electric field in LAO. As can be seen from the layer-resolved DOS shown in Figure 2c, the electric potential of the p-type LAO/STO changes along with the LAO thickness. The insulating-to-metallic transition critical thickness of p-type LAO/STO with one ML H_2O can be seen from Figure 2e. We obtain the energy of SEBM and CBM from the band structures of one ML H_2O on p-type LAO/STO with one to nine uc LAO. (Band structures of one ML H_2O on p-type LAO/STO with one to eight uc LAO are shown in Figure S3 in the Supporting Information.) When the energy of CBM is below VBM, which is set as the energy reference, the critical

DOI: 10.1021/acs.jpclett.8b00938
J. Phys. Chem. Lett. 2018, 9, 3049−3056

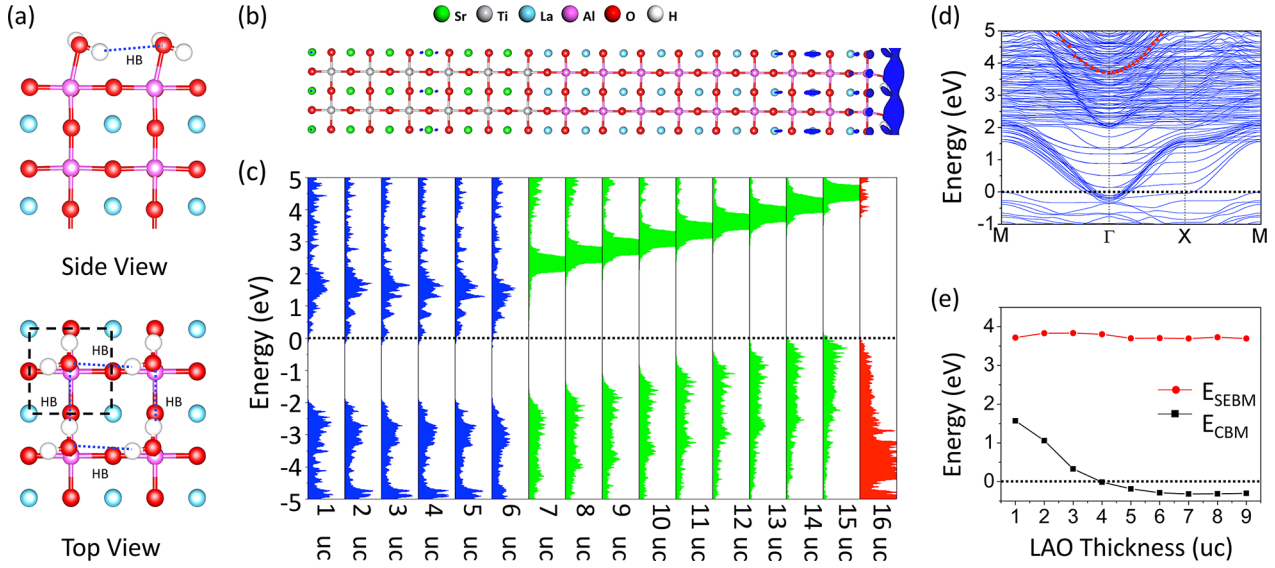

Figure 3. (a) Side and top views of H_2O adsorbed on n-type LAO/STO heterostructure. (b) Spatial orbital distribution of the solvated state in the H_2O layer. (c) DOS for every LAO, STO, and H_2O layer, represented by the green, blue, and cyan shades. The dashed line represents the position of E_F. (d) Band structure of one ML H_2O adsorbed on n-type LAO/STO. The solvated electron band is marked by red color. (e) Correlation of SEBM and CBM energies with LAO thickness. The energy of VBM is set as the reference in panels c−e. The results in panels a−d correspond to one ML H_2O adsorbed on n-type LAO/STO with nine uc's LAO. The E_F and VBM are very close in energy in panels c and d.

thickness is reached. With H_2O adsorption, the critical thickness of p-type LAO/STO increases from six to eight uc's, which is due to the vertical dipole moment induced by OH on La atom. Figure 2e shows that the energy of SEBM decreases from 3.6 to −0.03 eV with respect to the VBM with the increase in the LAO thickness. The CBM is contributed by the SEBM if the LAO is thicker than four uc's. Furthermore, the decrease in the SEBM energy correlates with the LAO thickness almost linearly before the thickness reaches the critical thickness of eight uc's. After reaching the critical thickness, the insulating-to-metallic transition occurs, and the electric potential stops increasing due to the interfacial charge transfer. This explains why the energy of SEBM becomes pinned at E_F.

The direction of built-in electric field in n-type LAO/STO is opposite to that of p-type heterostructure, and thus we expect to see a different influence on the solvated electron states. The LAO/STO heterostructure with n-type interface is terminated by AlO_2. Similar to the p-type interface, the H_2O adsorption structures also do not show significant dependence on the LAO thickness. H_2O adsorbs molecularly on the surface Al atom with an adsorption energy of 0.90 eV. The geometric and electronic structures of one ML H_2O on n-type LAO/STO with nine uc's LAO are shown in Figure 3a−d. There are two weak intermolecular HBs with bond lengths of 2.96 and 2.98 Å formed in one uc, and thus the solvated electron states can be bonded to the hydrogen atoms in the H_2O layer. The solvated electron band is shown in Figure 3d. The SEBM is 4.0 eV above the CBM with $m^* = 0.96m_e$, suggesting that the dispersive character of solvated electron band is preserved. The orbital distribution of SEBM is shown in Figure 3b. In this case, H_2O is almost parallel to the surface, and therefore the solvated electron states are mostly bound to the parallel rather than the vertical dipole moment. In contrast with the p-type LAO/STO, the SEBM on n-type LAO/STO is pushed to a higher energy due to the opposite direction of the internal electric field if we take CBM as the reference. It can be tuned from 2.1 to 4.0 eV relative to CBM, as shown in Figure 3e. We obtain the energy of SEBM and CBM from the band structures of one ML H_2O on n-type LAO/STO with one to nine uc LAO. (Band structures of one ML H_2O on n-type LAO/STO with one to eight uc LAO are shown in Figure S4 in the Supporting Information.) The energy of solvated electron states increases along with the LAO thickness up to 4.0 eV above CBM and remains fixed at this value for LAO thickness larger than the critical thickness (four uc's in this system). The VBM of this system is contributed by LAO, and it also increases along with the LAO thickness. Therefore, if taking VBM as reference, then the energy of SEBM remains around 3.7 eV.

Contrasting the solvated electron states on n and p types, the energy of the solvated electron state on p-type can be stabilized by increasing the LAO thickness from 3.6 to −0.03 eV compared with VBM, whereas the state can be tuned from 2.1 to 4.0 eV compared with CBM for n-type interface. This can be reasoned due to two factors. First, the critical thickness of p-type LAO/STO with H_2O adsorbates (eight uc's) is larger than the n-type system (four uc's), which allows the electric potential in LAO to reach a larger value in p-type LAO/STO. Second, the effective stabilization is also contributed by the vertical dipole moment of H_2O layer on LaO surface of p-type LAO/STO. The solvated electron is bound by such vertical dipole moment because it is in the same direction of electric potential in LAO. Therefore, the change of electric potential in LAO can easily affect the energy of solvated electron states. In contrast, in n-type of LAO/STO, the solvated electron states are mostly bound by the parallel dipole moment. In this case, the electric potential in LAO is less effective.

The p-type LAO/STO interface can successfully stabilize the solvated electron states. However, the SEBM is still above the CBM when LAO is thinner than four uc's, as can be seen from Figure 2e. In this case, similar to H_2O on TiO_2 surface, the electrons excited to the solvated electron states will transfer back to the LAO/STO surface within a certain lifetime. The

DOI: 10.1021/acs.jpclett.8b00938
J. Phys. Chem. Lett. 2018, 9, 3049−3056

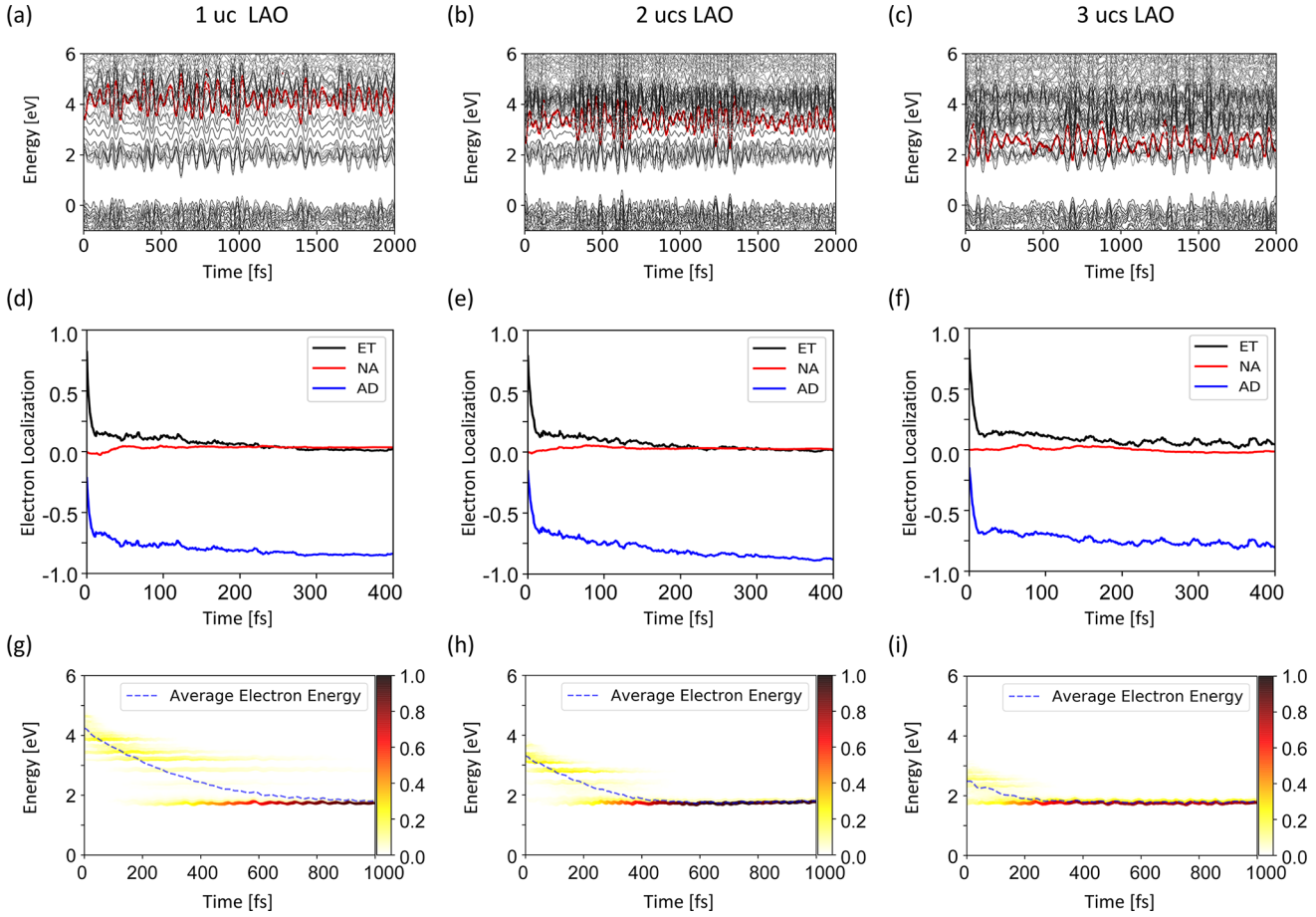

Figure 4. Charge-transfer dynamics of solvated electron of one ML H_2O adsorbed on p-type of LAO/STO with one to three uc LAO. (a–c) Time-dependent energy state evolution. The black (red) lines represent the energy levels contributed by LAO/STO (SEBM of H_2O). (d–f) Time-dependent electron localization projected onto the H_2O layer and p-type LAO/STO substrate. The total electron transfer (labeled as ET with black line) and the AD and NA contributions (blue and red lines) to the charge transfer are also plotted. (g–i) Time-dependent electron energy change. The energy of VBM is set as the reference in panels a–c and g–i.

charge-transfer dynamics of the solvated electrons are investigated using ab initio NAMD. The time-dependent energy state evolution is shown in Figure 4a–c for one to three uc LAO. The time-dependent electron transfer between the solvated electron states and LAO/STO can be obtained from NAMD calculations by initially exciting the electron into SEBM and then projecting the time-dependent electron localization onto the H_2O layer and LAO/STO substrate, as shown in Figure 4d–f. Moreover, the time-dependent electron-energy change can also be deduced by evaluating the electron probability distribution for selected energy states from the NAMD, as shown in Figure 4g–i. One can see that with one to three uc LAO, the localization of excited electron on H_2O layer decreases from ~80% to 15% within the first 15 fs. After that, it slowly decays to around zero within 1 ps. The ultrafast charge transfer (~15 fs) corresponds to the charge transfer from SEBM to LAO, whereas the slower transfer (<1 ps) corresponds to the charge transfer from LAO to STO, which contributes the CBM. The time-dependent electron energy change shows that the time scale for electron decay from SEBM to CBM decreases along with the energy of SEBM. With one uc LAO, it takes 1 ps for electron decay from SEBM to CBM, while for three uc's LAO, it takes only 300 fs.

Both the adiabatic (AD) and nonadiabatic (NA) mechanisms can contribute to the charge-transfer dynamics. During a molecular dynamics trajectory, AD charge transfer is provoked by nuclear motion, where transfer probability increases as the nuclear motion causes energy states to cross. By contrast, NA charge transfer involves direct charge hopping or tunneling between different states. These two mechanisms can be distinguished as described in the Supporting Information. Our analysis shows that the ultrafast charge transfer from SEBM to LAO/STO is mostly due to the AD charge-transfer mechanism. Here the AD charge transfer occurs when the SEBM crosses the LAO states frequently, and in these cases the hybridization between SEBM with LAO is significant, as shown in Figure 4a–c. This is because there is a high DOS contributed by LAO at the energy of the SEBM of adsorbed H_2O layer. The ultrafast charge-transfer behavior (in 15 fs time scale) for solvated electrons on LAO/STO with one to three uc LAO is similar to that on TiO_2 surface.[6,89] Photocatalytic reactions are typically difficult to happen within such a short time. However, if LAO is thicker than four uc's, as shown in Figure 2e, then the CBM is contributed by the SEBM and thus it can have much longer lifetime, which is comparable to the electron–hole recombination time scale in semiconductors.[83,90−92] When the LAO thickness reaches eight uc's, which is the critical thickness for insulating-to-metallic transition, the solvated electrons can be stabilized at E_F.

DOI: 10.1021/acs.jpclett.8b00938
J. Phys. Chem. Lett. 2018, 9, 3049−3056

We propose that the method of tuning solvated electron energy and dynamics using built-in electric field in the polar−nonpolar LAO/STO heterostructure is general and can be applied to other polar−nonpolar oxide heterostructures as well as ferroelectric systems. The flexibility of combining different polar−nonpolar oxides provides abundant choices. For example, the nonpolar STO can be replaced by TiO_2, and they can combine with another polar metal oxide like $LaVO_3$ or $GdTiO_3$.[93,94] For different polar−nonpolar heterostructures, the critical thickness and built-in electric potential can be different. Therefore, the tunability of the solvated electron states is different. On ferroelectric oxides, the direction and magnitude of the built-in electric field can be modulated by external electric field or temperature,[95] and therefore the energy and dynamics of solvated electron states can be tuned along with it.

In summary, we propose a strategy to tune the solvated electron states using the built-in electric field in the polar−nonpolar heterostructure. Taking LAO/STO and one ML H_2O as a prototypical system, it is found that the energy of the solvated electron state in H_2O can be significantly tuned by the built-in electric field in LAO. When H_2O molecules adsorb on p-type LAO/STO, the solvated electron states can be stabilized below E_F and be even partially occupied when the LAO is thicker than eight unit cells. The method of tuning solvated electron energy at oxide/aqueous interface using the built-in electric field in LAO/STO is proposed to be widely applicable to different polar−nonpolar systems as well as ferroelectric systems.

■ ASSOCIATED CONTENT

Supporting Information

The Supporting Information is available free of charge on the ACS Publications website at DOI: 10.1021/acs.jpclett.8b00938.

Computational details of ab initio NAMD and the adsorption energy (PDF)

■ AUTHOR INFORMATION

Corresponding Authors

*Q.Z.: E-mail: zqj@mail.ustc.edu.cn.
*J.Z.: E-mail: zhaojin@ustc.edu.cn.

ORCID

Qijing Zheng: 0000-0003-0022-3442
Wissam A. Saidi: 0000-0001-6714-4832
Jin Zhao: 0000-0003-1346-5280

Notes

The authors declare no competing financial interest.

■ ACKNOWLEDGMENTS

J.Z. acknowledges the support of the Ministry of Science and Technology of China, grant nos. 2016YFA0200604 and 2017YFA0204904; National Natural Science Foundation of China, grant nos. 11620101003 and 21421063; the Fundamental Research Funds for the Central Universities WK3510000005; and the U.S. National Science Foundation, grant no. CHE-1213189. Q.Z. acknowledges the support of National Natural Science Foundation of China, grant no. 11704363. W.A.S. acknowledges a start-up grant from the Department of Mechanical Engineering and Materials Science at the University of Pittsburgh. Calculations were performed in part at Environmental Molecular Sciences Laboratory at the PNNL, a user facility sponsored by the DOE Office of Biological and Environmental Research, Supercomputing Center at USTC, and Argonne Leadership Computing Facility, which is a DOE Office of Science User Facility supported under contract DE-AC02-06CH11357.

■ REFERENCES

(1) Kim, K. S.; Park, I. J.; Lee, S.; Cho, K.; Lee, J. Y.; Kim, J.; Joannopoulos, J. D. The Nature of a Wet Electron. *Phys. Rev. Lett.* **1996**, *76*, 956−959.

(2) Bragg, A. E.; Verlet, J. R. R.; Kammrath, A.; Cheshnovsky, O.; Neumark, D. M. Hydrated Electron Dynamics: From Clusters to Bulk. *Science* **2004**, *306*, 669−671.

(3) Hammer, N. I.; Shin, J.-W.; Headrick, J. M.; Diken, E. G.; Roscioli, J. R.; Weddle, G. H.; Johnson, M. A. How Do Small Water Clusters Bind an Excess Electron? *Science* **2004**, *306*, 675−679.

(4) Jordan, K. D. A Fresh Look at Electron Hydration. *Science* **2004**, *306*, 618−619.

(5) Paik, D. H.; Lee, I. R.; Yang, D. S.; Baskin, J. S.; Zewail, A. H. Electrons in Finite-Sized Water Cavities: Hydration Dynamics Observed in Real Time. *Science* **2004**, *306*, 672−675.

(6) Onda, K.; Li, B.; Zhao, J.; Jordan, K. D.; Yang, J.; Petek, H. Wet Electrons at the $H_2O/TiO_2(110)$ Surface. *Science* **2005**, *308*, 1154−1158.

(7) Verlet, J. R.; Bragg, A. E.; Kammrath, A.; Cheshnovsky, O.; Neumark, D. M. Observation of Large Water-Cluster Anions with Surface-Bound Excess Electrons. *Science* **2005**, *307*, 93−96.

(8) Zhao, J.; Li, B.; Onda, K.; Feng, M.; Petek, H. Solvated Electrons on Metal Oxide Surfaces. *Chem. Rev.* **2006**, *106*, 4402−4427.

(9) Larsen, R. E.; Glover, W. J.; Schwartz, B. J. Does the Hydrated Electron Occupy a Cavity? *Science* **2010**, *329*, 65−69.

(10) Marsalek, O.; Uhlig, F.; Frigato, T.; Schmidt, B.; Jungwirth, P. Dynamics of Electron Localization in Warm Versus Cold Water Clusters. *Phys. Rev. Lett.* **2010**, *105*, 043002.

(11) Siefermann, K. R.; Liu, Y.; Lugovoy, E.; Link, O.; Faubel, M.; Buck, U.; Winter, B.; Abel, B. Binding Energies, Lifetimes and Implications of Bulk and Interface Solvated Electrons in Water. *Nat. Chem.* **2010**, *2*, 274−279.

(12) Jacobson, L. D.; Herbert, J. M. Theoretical Characterization of Four Distinct Isomer Types in Hydrated-Electron Clusters, and Proposed Assignments for Photoelectron Spectra of Water Cluster Anions. *J. Am. Chem. Soc.* **2011**, *133*, 19889−19899.

(13) Alexander, W. A.; Wiens, J. P.; Minton, T. K.; Nathanson, G. M. Reactions of Solvated Electrons Initiated by Sodium Atom Ionization at the Vacuum-Liquid Interface. *Science* **2012**, *335*, 1072−1075.

(14) Wang, Z.; Liu, J.; Zhang, M.; Cukier, R. I.; Bu, Y. Solvation and Evolution Dynamics of an Excess Electron in Supercritical CO_2. *Phys. Rev. Lett.* **2012**, *108*, 207601.

(15) Elkins, M. H.; Williams, H. L.; Shreve, A. T.; Neumark, D. M. Relaxation Mechanism of the Hydrated Electron. *Science* **2013**, *342*, 1496−1499.

(16) Muller, E. A.; Strader, M. L.; Johns, J. E.; Yang, A.; Caplins, B. W.; Shearer, A. J.; Suich, D. E.; Harris, C. B. Femtosecond Electron Solvation at the Ionic Liquid/Metal Electrode Interface. *J. Am. Chem. Soc.* **2013**, *135*, 10646−10653.

(17) Yamamoto, Y.; Suzuki, Y.; Tomasello, G.; Horio, T.; Karashima, S.; Mitric, R.; Suzuki, T. Time- and Angle-Resolved Photoemission Spectroscopy of Hydrated Electrons near a Liquid Water Surface. *Phys. Rev. Lett.* **2014**, *112*, 187603.

(18) Stahler, J.; Deinert, J. C.; Wegkamp, D.; Hagen, S.; Wolf, M. Real-Time Measurement of the Vertical Binding Energy During the Birth of a Solvated Electron. *J. Am. Chem. Soc.* **2015**, *137*, 3520−3524.

(19) Coons, M. P.; You, Z. Q.; Herbert, J. M. The Hydrated Electron at the Surface of Neat Liquid Water Appears to Be Indistinguishable from the Bulk Species. *J. Am. Chem. Soc.* **2016**, *138*, 10879−10886.

(20) Karashima, S.; Yamamoto, Y.; Suzuki, T. Resolving Non-adiabatic Dynamics of Hydrated Electrons Using Ultrafast Photoemission Anisotropy. *Phys. Rev. Lett.* **2016**, *116*, 137601.

DOI: 10.1021/acs.jpclett.8b00938
J. Phys. Chem. Lett. 2018, 9, 3049−3056

(21) Hartweg, S.; Yoder, B. L.; Garcia, G. A.; Nahon, L.; Signorell, R. Size-Resolved Photoelectron Anisotropy of Gas Phase Water Clusters and Predictions for Liquid Water. *Phys. Rev. Lett.* **2017**, *118*, 103402.
(22) Ellis, J. L.; Hickstein, D. D.; Xiong, W.; Dollar, F.; Palm, B. B.; Keister, K. E.; Dorney, K. M.; Ding, C.; Fan, T.; Wilker, M. B.; et al. Materials Properties and Solvated Electron Dynamics of Isolated Nanoparticles and Nanodroplets Probed with Ultrafast Extreme Ultraviolet Beams. *J. Phys. Chem. Lett.* **2016**, *7*, 609−615.
(23) Zhang, C.; Luo, Q.; Cheng, S.; Bu, Y. Unusual Indirect Nuclear Spin-Spin Exchange Coupling through Solvated Electron. *J. Phys. Chem. Lett.* **2018**, *9*, 689.
(24) West, A. H.; Yoder, B. L.; Luckhaus, D.; Saak, C.-M.; Doppelbauer, M.; Signorell, R. Angle-Resolved Photoemission of Solvated Electrons in Sodium-Doped Clusters. *J. Phys. Chem. Lett.* **2015**, *6*, 1487−1492.
(25) Le Caër, S.; Ortiz, D.; Marignier, J.-L.; Schmidhammer, U.; Belloni, J.; Mostafavi, M. Ultrafast Decay of the Solvated Electron in a Neat Polar Solvent: The Unusual Case of Propylene Carbonate. *J. Phys. Chem. Lett.* **2016**, *7*, 186−190.
(26) Šmídová, D.; Lengyel, J.; Pysanenko, A.; Med, J.; Slavíček, P.; Fárník, M. Reactivity of Hydrated Electron in Finite Size System: Sodium Pickup on Mixed N_2O−Water Nanoparticles. *J. Phys. Chem. Lett.* **2015**, *6*, 2865−2869.
(27) Ariyarathna, I. R.; Khan, S. N.; Pawłowski, F.; Ortiz, J. V.; Miliordos, E. Aufbau Rules for Solvated Electron Precursors: $Be(NH_3)_4^{0,\pm}$ Complexes and Beyond. *J. Phys. Chem. Lett.* **2018**, *9*, 84−88.
(28) Casey, J. R.; Schwartz, B. J.; Glover, W. J. Free Energies of Cavity and Noncavity Hydrated Electrons near the Instantaneous Air/Water Interface. *J. Phys. Chem. Lett.* **2016**, *7*, 3192−3198.
(29) Li, B.; Yu, J. P.; Brunzelle, J. S.; Moll, G. N.; van der Donk, W. A.; Nair, S. K. Structure and Mechanism of the Lantibiotic Cyclase Involved in Nisin Biosynthesis. *Science* **2006**, *311*, 1464−1467.
(30) Lan, Z.; Frutos, L. M.; Sobolewski, A. L.; Domcke, W. Photochemistry of Hydrogen-Bonded Aromatic Pairs: Quantum Dynamical Calculations for the Pyrrole-Pyridine Complex. *Proc. Natl. Acad. Sci. U. S. A.* **2008**, *105*, 12707−12712.
(31) Petek, H.; Zhao, J. Ultrafast Interfacial Proton-Coupled Electron Transfer. *Chem. Rev.* **2010**, *110*, 7082−7099.
(32) Lim, C. H.; Holder, A. M.; Musgrave, C. B. Mechanism of Homogeneous Reduction of CO_2 by Pyridine: Proton Relay in Aqueous Solvent and Aromatic Stabilization. *J. Am. Chem. Soc.* **2013**, *135*, 142−154.
(33) Zhu, D.; Zhang, L. H.; Ruther, R. E.; Hamers, R. J. Photo-Illuminated Diamond as a Solid-State Source of Solvated Electrons in Water for Nitrogen Reduction. *Nat. Mater.* **2013**, *12*, 836−841.
(34) Ufimtsev, I. S.; Luehr, N.; Martinez, T. J. Charge Transfer and Polarization in Solvated Proteins from Ab Initio Molecular Dynamics. *J. Phys. Chem. Lett.* **2011**, *2*, 1789−1793.
(35) Nguyen, P. D.; Ding, F.; Fischer, S. A.; Liang, W.; Li, X. Solvated First-Principles Excited-State Charge-Transfer Dynamics with Time-Dependent Polarizable Continuum Model and Solvent Dielectric Relaxation. *J. Phys. Chem. Lett.* **2012**, *3*, 2898−2904.
(36) Iglev, H.; Kolev, S. K.; Rossmadl, H.; Petkov, P. S.; Vayssilov, G. N. Hydrogen Atom Transfer from Water or Alcohols Activated by Presolvated Electrons. *J. Phys. Chem. Lett.* **2015**, *6*, 986−992.
(37) Alizadeh, E.; Sanz, A. G.; García, G.; Sanche, L. Radiation Damage to DNA: The Indirect Effect of Low-Energy Electrons. *J. Phys. Chem. Lett.* **2013**, *4*, 820−825.
(38) Oliver, T. A.; Zhang, Y.; Roy, A.; Ashfold, M. N.; Bradforth, S. E. Exploring Autoionization and Photoinduced Proton-Coupled Electron Transfer Pathways of Phenol in Aqueous Solution. *J. Phys. Chem. Lett.* **2015**, *6*, 4159−4164.
(39) Nowakowski, P. J.; Woods, D. A.; Verlet, J. R. Charge Transfer to Solvent Dynamics at the Ambient Water/Air Interface. *J. Phys. Chem. Lett.* **2016**, *7*, 4079−4085.
(40) Ma, J.; Schmidhammer, U.; Mostafavi, M. Direct Evidence for Transient Pair Formation between a Solvated Electron and H_3O^+ Observed by Picosecond Pulse Radiolysis. *J. Phys. Chem. Lett.* **2014**, *5*, 2219−2223.
(41) Uhlig, F.; Marsalek, O.; Jungwirth, P. Unraveling the Complex Nature of the Hydrated Electron. *J. Phys. Chem. Lett.* **2012**, *3*, 3071−3075.
(42) Bragg, A. E.; Kanu, G. U.; Schwartz, B. J. Nanometer-Scale Phase Separation and Preferential Solvation in THF−Water Mixtures: Ultrafast Electron Hydration and Recombination Dynamics Following CTTS Excitation of I^-. *J. Phys. Chem. Lett.* **2011**, *2*, 2797−2804.
(43) Doan, S. C.; Schwartz, B. J. Nature of Excess Electrons in Polar Fluids: Anion-Solvated Electron Equilibrium and Polarized Hole-Burning in Liquid Acetonitrile. *J. Phys. Chem. Lett.* **2013**, *4*, 1471−1476.
(44) Ambrosio, F.; Miceli, G.; Pasquarello, A. Electronic Levels of Excess Electrons in Liquid Water. *J. Phys. Chem. Lett.* **2017**, *8*, 2055−2059.
(45) Jordan, K. D.; Wang, F. Theory of Dipole-Bound Anions. *Annu. Rev. Phys. Chem.* **2003**, *54*, 367−396.
(46) Lee, S.; Kim, J.; Lee, S. J.; Kim, K. S. Novel Structures for the Excess Electron State of the Water Hexamer and the Interaction Forces Governing the Structures. *Phys. Rev. Lett.* **1997**, *79*, 2038−2041.
(47) Zhan, C. G.; Dixon, D. A. The Nature and Absolute Hydration Free Energy of the Solvated Electron in Water. *J. Phys. Chem. B* **2003**, *107*, 4403−4417.
(48) Bovensiepen, U.; Gahl, C.; Stahler, J.; Bockstedte, M.; Meyer, M.; Baletto, F.; Scandolo, S.; Zhu, X. Y.; Rubio, A.; Wolf, M. A Dynamic Landscape from Femtoseconds to Minutes for Excess Electrons at Ice-Metal Interfaces. *J. Phys. Chem. C* **2009**, *113*, 979−988.
(49) Bovensiepen, U.; Gahl, C.; Wolf, M. Solvation Dynamics and Evolution of the Spatial Extent of Photoinjected Electrons in D_2O/Cu(111). *J. Phys. Chem. B* **2003**, *107*, 8706−8715.
(50) Gahl, C.; Bovensiepen, U.; Frischkorn, C.; Wolf, M. Ultrafast Dynamics of Electron Localization and Solvation in Ice Layers on Cu(111). *Phys. Rev. Lett.* **2002**, *89*, 107402.
(51) Stähler, J.; Bovensiepen, U.; Meyer, M.; Wolf, M. A Surface Science Approach to Ultrafast Electron Transfer and Solvation Dynamics at Interfaces. *Chem. Soc. Rev.* **2008**, *37*, 2180−2190.
(52) Stahler, J.; Mehlhorn, M.; Bovensiepen, U.; Meyer, M.; Kusmierek, D. O.; Morgenstern, K.; Wolf, M. Impact of Ice Structure on Ultrafast Electron Dynamics in D_2O Clusters on Cu(111). *Phys. Rev. Lett.* **2007**, *98*, 206105.
(53) Li, B.; Zhao, J.; Onda, K.; Jordan, K. D.; Yang, J.; Petek, H. Ultrafast Interfacial Proton-Coupled Electron Transfer. *Science* **2006**, *311*, 1436−1440.
(54) Zhao, J.; Li, B.; Jordan, K. D.; Yang, J.; Petek, H. Interplay between Hydrogen Bonding and Electron Solvation on Hydrated TiO_2(110). *Phys. Rev. B: Condens. Matter Mater. Phys.* **2006**, *73*, 195309.
(55) Zhao, J.; Yang, J.; Petek, H. Theoretical Study of the Molecular and Electronic Structure of Methanol on a TiO_2(110) Surface. *Phys. Rev. B: Condens. Matter Mater. Phys.* **2009**, *80*, 235416.
(56) Koitaya, T.; Nakamura, H.; Yamashita, K. First-Principle Calculations of Solvated Electrons at Protic Solvent−TiO_2 Interfaces with Oxygen Vacancies. *J. Phys. Chem. C* **2009**, *113*, 7236−7245.
(57) Migani, A.; Mowbray, D. J.; Iacomino, A.; Zhao, J.; Petek, H.; Rubio, A. Level Alignment of a Prototypical Photocatalytic System: Methanol on TiO_2(110). *J. Am. Chem. Soc.* **2013**, *135*, 11429−11432.
(58) Migani, A.; Mowbray, D. J.; Zhao, J.; Petek, H.; Rubio, A. Quasiparticle Level Alignment for Photocatalytic Interfaces. *J. Chem. Theory Comput.* **2014**, *10*, 2103−2113.
(59) Bert, J. A.; Kalisky, B.; Bell, C.; Kim, M.; Hikita, Y.; Hwang, H. Y.; Moler, K. A. Direct Imaging of the Coexistence of Ferromagnetism and Superconductivity at the $LaAlO_3/SrTiO_3$ Interface. *Nat. Phys.* **2011**, *7*, 767−771.
(60) Cancellieri, C.; Fontaine, D.; Gariglio, S.; Reyren, N.; Caviglia, A.; Fete, A.; Leake, S.; Pauli, S.; Willmott, P.; Stengel, M.; et al.

DOI: 10.1021/acs.jpclett.8b00938
J. Phys. Chem. Lett. 2018, 9, 3049−3056

Electrostriction at the $LaAlO_3/SrTiO_3$ Interface. *Phys. Rev. Lett.* **2011**, *107*, 056102.
(61) Caviglia, A. D.; Gariglio, S.; Reyren, N.; Jaccard, D.; Schneider, T.; Gabay, M.; Thiel, S.; Hammerl, G.; Mannhart, J.; Triscone, J. M. Electric Field Control of the $LaAlO_3/SrTiO_3$ Interface Ground State. *Nature* **2008**, *456*, 624−627.
(62) Guo, H.; Saidi, W. A.; Yang, J.; Zhao, J. Nano-Scale Polar-Nonpolar Oxide Heterostructures for Photocatalysis. *Nanoscale* **2016**, *8*, 6057−6063.
(63) Guo, H. L.; Saidi, W. A.; Zhao, J. Tunability of the Two-Dimensional Electron Gas at the $LaAlO_3/SrTiO_3$ Interface by Strain-Induced Ferroelectricity. *Phys. Chem. Chem. Phys.* **2016**, *18*, 28474−28484.
(64) Lee, J.-S.; Xie, Y.; Sato, H.; Bell, C.; Hikita, Y.; Hwang, H.; Kao, C.-C. Titanium d_{xy} Ferromagnetism at the $LaAlO_3/SrTiO_3$ Interface. *Nat. Mater.* **2013**, *12*, 703−706.
(65) Liang, H. X.; Cheng, L.; Zhai, X. F.; Pan, N.; Guo, H. L.; Zhao, J.; Zhang, H.; Li, L.; Zhang, X. Q.; Wang, X. P.; et al. Giant Photovoltaic Effects Driven by Residual Polar Field within Unit-Cell-Scale $LaAlO_3$ Films on $SrTiO_3$. *Sci. Rep.* **2013**, *3*, 1975.
(66) Nakagawa, N.; Hwang, H. Y.; Muller, D. A. Why Some Interfaces Cannot Be Sharp. *Nat. Mater.* **2006**, *5*, 204−209.
(67) Ohtomo, A.; Hwang, H. Y. A High-Mobility Electron Gas at the $LaAlO_3/SrTiO_3$ Heterointerface. *Nature* **2004**, *427*, 423−426.
(68) Pentcheva, R.; Pickett, W. E. Avoiding the Polarization Catastrophe in $LaAlO_3$ Overlayers on $SrTiO_3(001)$ through Polar Distortion. *Phys. Rev. Lett.* **2009**, *102*, 107602.
(69) Reinle-Schmitt, M. L.; Cancellieri, C.; Li, D.; Fontaine, D.; Medarde, M.; Pomjakushina, E.; Schneider, C. W.; Gariglio, S.; Ghosez, P.; Triscone, J. M.; et al. Tunable Conductivity Threshold at Polar Oxide Interfaces. *Nat. Commun.* **2012**, *3*, 932.
(70) Shalom, M. B.; Sachs, M.; Rakhmilevitch, D.; Palevski, A.; Dagan, Y. Tuning Spin-Orbit Coupling and Superconductivity at the $SrTiO_3/LaAlO_3$ Interface: A Magnetotransport Study. *Phys. Rev. Lett.* **2010**, *104*, 126802.
(71) Singh-Bhalla, G.; Bell, C.; Ravichandran, J.; Siemons, W.; Hikita, Y.; Salahuddin, S.; Hebard, A. F.; Hwang, H. Y.; Ramesh, R. Built-in and Induced Polarization across $LaAlO_3/SrTiO_3$ Heterojunctions. *Nat. Phys.* **2011**, *7*, 80−86.
(72) Thiel, S.; Hammerl, G.; Schmehl, A.; Schneider, C. W.; Mannhart, J. Tunable Quasi-Two-Dimensional Electron Gases in Oxide Heterostructures. *Science* **2006**, *313*, 1942−1945.
(73) Xie, Y.; Bell, C.; Yajima, T.; Hikita, Y.; Hwang, H. Y. Charge Writing at the $LaAlO_3/SrTiO_3$ Surface. *Nano Lett.* **2010**, *10*, 2588−2591.
(74) Evarestov, R.; Bandura, A.; Alexandrov, V. Adsorption of Water on (0 0 1) Surface of $SrTiO_3$ and $SrZrO_3$ Cubic Perovskites: Hybrid HF-DFT LCAO Calculations. *Surf. Sci.* **2007**, *601*, 1844−1856.
(75) Guhl, H.; Miller, W.; Reuter, K. Water Adsorption and Dissociation on $SrTiO_3(001)$ Revisited: A Density Functional Theory Study. *Phys. Rev. B: Condens. Matter Mater. Phys.* **2010**, *81*, 155455.
(76) Holmstrom, E.; Spijker, P.; Foster, A. S. The Interface of $SrTiO_3$ and H_2O from Density Functional Theory Molecular Dynamics. *Proc. R. Soc. London, Ser. A* **2016**, *472*, 20160293.
(77) Kresse, G.; Hafner, J. Ab Initio Molecular Dynamics for Liquid Metals. *Phys. Rev. B: Condens. Matter Mater. Phys.* **1993**, *47*, 558−561.
(78) Kresse, G.; Hafner, J. Ab Initio Molecular Dynamics for Open-Shell Transition Metals. *Phys. Rev. B: Condens. Matter Mater. Phys.* **1993**, *48*, 13115−13118.
(79) Kresse, G.; Hafner, J. Ab-Initio Molecular-Dynamics Simulation of the Liquid-Metal Amorphous-Semiconductor Transition in Germanium. *Phys. Rev. B: Condens. Matter Mater. Phys.* **1994**, *49*, 14251−14269.
(80) Perdew, J. P.; Burke, K.; Ernzerhof, M. Generalized Gradient Approximation Made Simple. *Phys. Rev. Lett.* **1996**, *77*, 3865−3868.
(81) Kresse, G.; Joubert, D. From Ultrasoft Pseudopotentials to the Projector Augmented-Wave Method. *Phys. Rev. B: Condens. Matter Mater. Phys.* **1999**, *59*, 1758−1775.
(82) Zheng, Q.; Saidi, W. A.; Xie, Y.; Lan, Z.; Prezhdo, O. V.; Petek, H.; Zhao, J. Phonon-Assisted Ultrafast Charge Transfer at Van Der Waals Heterostructure Interface. *Nano Lett.* **2017**, *17*, 6435−6442.
(83) Zhang, L.; Zheng, Q.; Xie, Y.; Lan, Z.; Prezhdo, O.; Saidi, W.; Zhao, J. Delocalized Impurity Phonon Induced Electron-Hole Recombination in Doped Semiconductor. *Nano Lett.* **2018**, *18*, 1592−1599.
(84) Akimov, A. V.; Prezhdo, O. V. The Pyxaid Program for Non-Adiabatic Molecular Dynamics in Condensed Matter Systems. *J. Chem. Theory Comput.* **2013**, *9*, 4959−4972.
(85) Akimov, A. V.; Prezhdo, O. V. Advanced Capabilities of the Pyxaid Program: Integration Schemes, Decoherence Effects, Multi-excitonic States, and Field-Matter Interaction. *J. Chem. Theory Comput.* **2014**, *10*, 789−804.
(86) Chu, W. B.; Saidi, W. A.; Zheng, Q. J.; Xie, Y.; Lan, Z. G.; Prezhdo, O. V.; Petek, H.; Zhao, J. Ultrafast Dynamics of Photongenerated Holes at a CH_3OH/TiO_2 Rutile Interface. *J. Am. Chem. Soc.* **2016**, *138*, 13740−13749.
(87) Migani, A.; Blancafort, L. Excitonic Interfacial Proton-Coupled Electron Transfer Mechanism in the Photocatalytic Oxidation of Methanol to Formaldehyde on $TiO_2(110)$. *J. Am. Chem. Soc.* **2016**, *138*, 16165−16173.
(88) Migani, A.; Blancafort, L. What Controls Photocatalytic Water Oxidation on Rutile $TiO_2(110)$ under Ultra-High-Vacuum Conditions? *J. Am. Chem. Soc.* **2017**, *139*, 11845−11856.
(89) Fischer, S. A.; Duncan, W. R.; Prezhdo, O. V. Ab Initio Nonadiabatic Molecular Dynamics of Wet-Electrons on the TiO_2 Surface. *J. Am. Chem. Soc.* **2009**, *131*, 15483−15491.
(90) Ozawa, K.; Emori, M.; Yamamoto, S.; Yukawa, R.; Yamamoto, S.; Hobara, R.; Fujikawa, K.; Sakama, H.; Matsuda, I. Electron-Hole Recombination Time at TiO_2 Single-Crystal Surfaces: Influence of Surface Band Bending. *J. Phys. Chem. Lett.* **2014**, *5*, 1953−1957.
(91) Wang, H.; Zhang, C.; Rana, F. Ultrafast Dynamics of Defect-Assisted Electron-Hole Recombination in Monolayer MoS_2. *Nano Lett.* **2015**, *15*, 339−345.
(92) Long, R.; English, N. J.; Prezhdo, O. V. Minimizing Electron-Hole Recombination on TiO_2 Sensitized with PbSe Quantum Dots: Time-Domain Ab Initio Analysis. *J. Phys. Chem. Lett.* **2014**, *5*, 2941−2946.
(93) Basey-Fisher, T.; Hanham, S.; Andresen, H.; Maier, S.; Stevens, M.; Alford, N.; Klein, N. Microwave Debye Relaxation Analysis of Dissolved Proteins: Towards Free-Solution Biosensing. *Appl. Phys. Lett.* **2011**, *99*, 233703.
(94) Moser, J.; Barreiro, A.; Bachtold, A. Current-Induced Cleaning of Graphene. *Appl. Phys. Lett.* **2007**, *91*, 163513.
(95) Dawber, M.; Rabe, K. M.; Scott, J. F. Physics of Thin-Film Ferroelectric Oxides. *Rev. Mod. Phys.* **2005**, *77*, 1083−1130.

DOI: 10.1021/acs.jpclett.8b00938
J. Phys. Chem. Lett. 2018, 9, 3049−3056